Journal of Materials Chemistry C

PAPER

View Article Online
View Journal | View Issue

Cite this: J. Mater. Chem. C, 2015, 3, 596

Solution-assembled nanowires for high performance flexible and transparent solar-blind photodetectors

Jiangxin Wang,[a] Chaoyi Yan,[a] Meng-Fang Lin,[b] Kazuhito Tsukagoshi[b] and Pooi See Lee*[a]

Received 13th October 2014
Accepted 14th November 2014

DOI: 10.1039/c4tc02297a

www.rsc.org/MaterialsC

Solar-blind photodetectors based on Zn_2GeO_4 (ZGO) nanowires (NWs) with high transparency and good flexibility were successfully fabricated on a polyethylene terephthalate (PET) substrate using a facile all solution-processible method. The electrodes and functional channels are constructed with silver NWs (Ag NWs) and ZGO NWs, respectively, using a spray coating method. The spray-coated all-NW device exhibited high transparency, good mechanical bending stability, high photoresponse, and short cutoff wavelength. The Schottky barrier between the Ag–ZGO NWs together with the junction barrier between interconnecting ZGO NWs contributed to a high photoresponse and improved switching time in the devices. We propose that the unique energy band structure of the ZGO NW networks provides an additional mechanism to further reduce the cutoff wavelength in solar-blind photodetectors.

Introduction

Flexible and transparent electronic devices are of great interest for many emerging applications.[1–4] The capability to fabricate optically transparent and mechanically flexible electronic devices paves the way for the next-generation "see-through" and conformable devices. Solar-blind photodetectors which detect light in the spectral range of 190–280 nm have important applications in biological threat detection, missile tracking, flame detection, ozone hole sensing, *etc.*[5–7] Flexible and meanwhile transparent solar-blind photodetectors enable the integration of wearable monitoring and sensing systems on top of other devices without affecting the visibility of the devices beneath. NWs are promising building blocks for these devices. They possess inherent mechanical flexibility and can be easily coated onto arbitrary substrates by inkjet printing, spin coating, drop casting or spray coating methods, *etc.*, meeting the prospects of large-area processability and low-temperature compatibility with most of the flexible substrates. The prototypical indium tin oxide (ITO) is normally used as the transparent electrode in transparent photodetectors while nanowires were used as the sensing materials.[8,9] Limited by the brittle nature and high temperature deposition process of the ITO electrode, the advantages of NW in large bending strain compliance and low-temperature processability could not be fully utilized. On the other hand, percolating metal NWs have recently attracted a great deal of interest for electrode applications and have been demonstrated to be promising alternatives due to their good conductivity, solution processability, high transparency and flexibility.[10–15] Among these materials, the Ag NW film is an outstanding candidate which offers good conductivity and transparency ($\sim$10 Ω sq^{-1} with 90% transmittance).

Semiconductor nanowires have been extensively studied for their applications in photodetectors.[16–23] It is widely recognized that the 1D nanostructure contributes to high photosensitivity due to the large surface-to-volume ratio which prolongs the lifetime of the photo-generated carriers with appreciable band bending on the nanowire surface. It is demonstrated in this report that the unique properties of NWs not only provide high photosensitivity to the NW photodetectors, but can also introduce an additional mechanism to reduce the photoresponse time and the cutoff wavelength of the photodetectors while being assembled into the network structure. Wide-bandgap semiconductor NWs are promising materials for solar-blind photodetectors. Their large bandgaps minimize the chance of false detection and reduce high background under infrared or visible light, eliminating the use of expensive and bulky optical filters. Recently, β-Ga_2O_3 nanostructures,[24,25] $In_2Ge_2O_7$ nanowires,[26] and Zn_2GeO_4 NWs[27,28] have been used as solar-blind light detection materials. However, these devices still showed certain photoresponse to the incident light with wavelength longer than 280 nm. Moreover, the fabrication approaches in these reports typically involved complicated lithography fabrication procedures. Efficient large-scale device fabrication of flexible and transparent NW solar-blind photodetectors is still lacking. Hereby, we report that with the use of a simple

[a]School of Materials Science and Engineering, Nanyang Technological University, 50 Nanyang Avenue, Singapore 639798. E-mail: pslee@ntu.edu.sg
[b]International Center for Materials Nanoarchitectonics (WPI-MANA), National Institute for Materials Science (NIMS), Tsukuba, Ibaraki 305-0044, Japan

solution-assembly method, high performance flexible and transparent solar-blind photodetectors can be fabricated. This method helps to tackle the aforementioned difficulties and full advantages of NWs in their large mechanical compliance and low temperature processability can be harvested.

Experimental

Device fabrication

ZGO NWs were grown on Si substrates by a chemical vapor deposition (CVD) method.[29] The NWs were removed from the substrates and dispersed in isopropyl alcohol (IPA) at a concentration of ~0.1 mg ml^{-1} with sonication for 15 min. The Ag NW solution was purchased from Seashell Technology with diameters of 120–150 nm and lengths of 20–50 μm. The concentration was diluted to 0.5 mg ml^{-1} in IPA before use. Fig. 1a illustrates the fabrication procedures of the flexible and transparent UV photodetectors. First, the ZGO NW solution was spray-coated onto the PET substrate through a shadow mask, forming light detection channels. Second, Ag NWs were coated analogously through another shadow mask, forming transparent and conductive percolating Ag NW network electrodes. The resultant photodetectors had a channel length of 0.15 mm and channel width of 1.2 mm. Two ml of ZGO NW solution and 1 ml of Ag NW solution were used to coat onto a substrate area of 2 × 2 cm. Due to the fast evaporation rate of IPA, no substrate heating is required during the spray-coating process.

Characterization

SEM images of the samples were taken with a field-emission SEM (FE-SEM, JSM 7600F). The X-ray diffraction patterns were measured on a Shimadzu XRD-6000 instrument with Cu Kα radiation. The transmittance spectra were recorded using a Shimadzu spectrometer (UV-2550). The electrical properties of the photodetector were characterized using a Keithley 4200-SCS parameter analyzer equipped with remote PreAmp models to enable low current measurement. The photoresponse of the device under different wavelengths was measured using a wavelength tunable monochromatic light source, which included a 150 W xenon lamp and an Omniλ-series monochromator with an output bandwidth of 0.2 nm. The bending test was carried out on a home-made translation stage. The photodetector performance was measured when the stage compressed the devices to different bending angles.

Results and discussion

Fig. 1b shows a schematic image of the flexible NW photodetector. The highly conductive Ag NW networks construct the transparent electrodes. The ZGO interconnecting NW networks were homogeneously dispersed on the substrate, located below the Ag NW electrodes as the solar-blind light detection channels. Five by five photodetector arrays were fabricated on a PET substrate. The photodetector shows excellent transparency with the letters clearly seen under the device, as shown in Fig. 1c. The photograph in Fig. 1d demonstrates a device under bending. The photodetector can be repetitively bent to an angle of 90° and released. No peeling or deformation of the device structures was observed after the bending. The haze appearance in the device is due to light scattering by the NW films.

The morphology of the Ag NWs and ZGO NWs is presented in Fig. 2a and b, respectively. A large amount of ZGO NWs on the silicon substrate could be synthesized by the CVD method (~10 mg nanowires on a 1 × 1.5 cm substrate). The nanowires were quite homogeneous and possessed a high aspect ratio with a diameter of ~100 nm and length typically around 100 μm. Fig. 2c shows the SEM image of the photodetector in the channel/electrode overlap region. The region on the right side

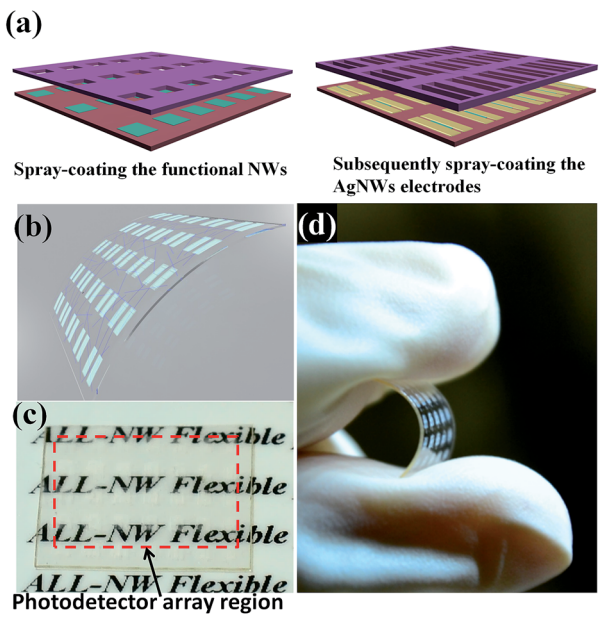

Fig. 1 (a) Schematic images of the device fabrication procedures. (b) A schematic image of the transparent and flexible photodetectors. (c and d) Photographs showing good transparency and flexibility of the device.

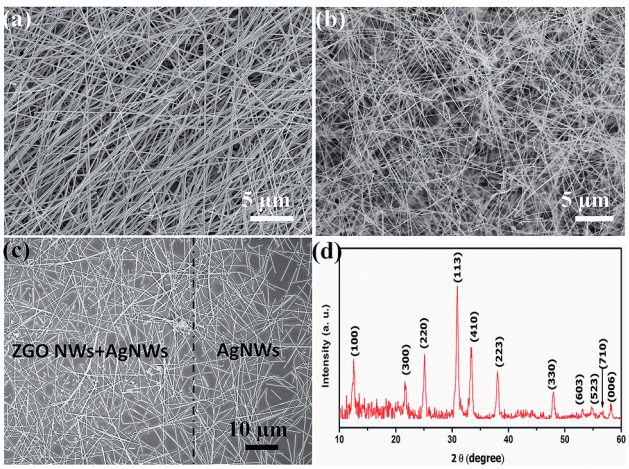

Fig. 2 Top SEM images of (a) Ag NWs, (b) ZGO NWs, and (c) ZGO NW and Ag NW interface region in the photodetector device. (d) XRD pattern of the ZGO NWs.

of the dashed line contains pure Ag NWs while the left region is the overlap between the electrode and detection channel which contains Ag NWs and ZGO NWs. The two types of NWs form percolating NW networks, establishing good connection between the device electrode and channel. The XRD patterns in Fig. 2d show that the NWs have a pure rhombohedral crystal phase (JCPDS: 011-0687, $a = 14.231$ Å and $b = 9.53$ Å). The high crystallinity nature of the ZGO NWs eliminates our concern of impurity which may affect the device performance. The ultra-high photoresponse behavior of the device can also be partially attributed to the high purity and good crystallinity of the ZGO NWs synthesized by the CVD method.

The device achieved a high transparency of ~80% transmittance in the visible light range with the transmittance of the pure PET substrate being 90%, as shown in Fig. 3a. The transmittance of the devices can be further improved by using the PET substrate with higher transparency. Due to light scattering by the NW networks, the device transmittance value might be underestimated as ultraviolet-visible spectroscopy in our experiment is not capable of measuring the scattered light transmitted through the device.[30] Fig. 3b illustrates the *I–V* curve of the devices under 250 nm UV light illumination and dark conditions. The asymmetric behavior in the *I–V* characteristic was attributed to the different contact conditions at the two sides of the electrodes.[27,28] The nonlinear *I–V* curve indicates the existence of energy barriers in the device. The dark current of the device is around 10 fA at 10 V bias. The extremely small dark current can be attributed to the low carrier intensity (1.78×10^{17} cm^{-3}, calculated by Liu *et al.*[31]) in the intrinsic ZGO NWs. In addition, both the Ag NW–ZGO NW Schottky barrier and ZGO NW–ZGO NW junction barrier contributed to further suppression of the dark current. The photocurrent of the device significantly increases to 30 pA while it is illuminated with UV light at 250 nm (~0.2 mW cm^{-2}), giving an on/off ratio of 3000. The on/off ratio is much higher compared to that of the reported UV photodetectors using ZGO NWs as the light detection materials (typically dozens of times[28,31–33]) and close to the best reported result which showed an on/off ratio of a few thousands of times on devices fabricated by an elaborate e-beam lithography method.[27] The photocurrent jumps to the maximum value immediately after the UV light is on, as shown in Fig. 3c. The device recovers to the dark current promptly after the UV light is off. The response time and reset time are below 5 s and 2.6 s, respectively. It should be noted that the switching time was limited by the fastest measurement time of the equipment which was prolonged by the extremely low dark current in the device. The response time is faster compared to that of the reported single ZGO NW photodetector (12 s).[27] The improved response time and high photoresponse are attributed to the Schottky barriers and NW junction barriers between the NW networks, as interpreted in Fig. 3e. The work function of Ag NWs is around 4.3 eV while the conduction band of ZGO NWs is located at around 3.8 eV. Mismatch in the energy levels leads to Schottky barrier formation at the Ag NW–ZGO NW interface. Band bending at the ZGO NW surface will also generate energy barriers at the ZGO NW junctions. It is understood that under light illumination, the Schottky barrier height will be lowered and its width will be narrowed.[34–36] Similar effects were also observed at the ZGO NW junction barriers in the network structure.[28] Modulation of the barrier height and width under light illumination is the dominant mechanism dictating the photocurrent transport behavior in the device. The carrier transport is mainly restricted at the energy barriers. The reduction of barrier height and width will lead to the gating effect which significantly increases the photocurrent. As the modulation only takes place at the interface instead of the whole NW surface, it provides a faster switching mechanism for the photodetectors.[35]

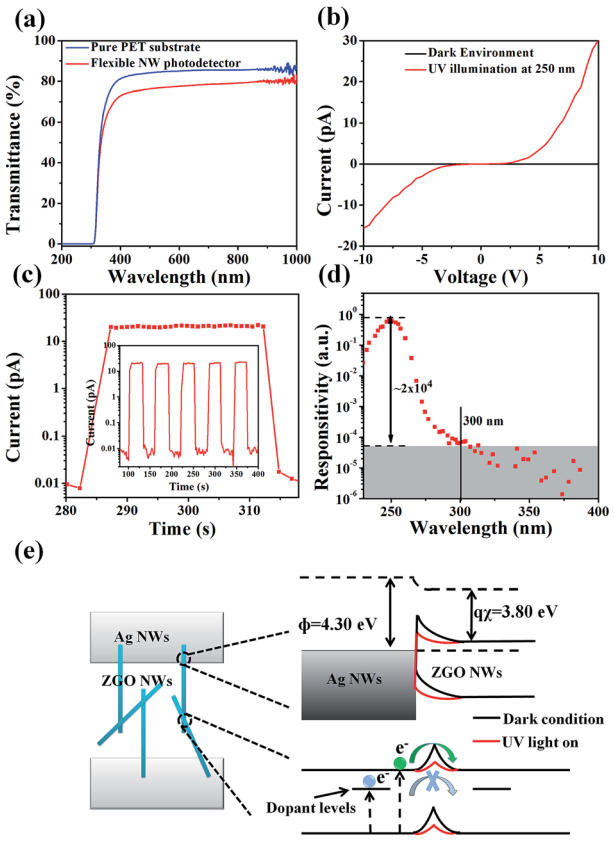

Fig. 3 (a) Transmittance spectra of the pure PET substrate and the flexible NW photodetector. (b) *I–V* curves of the photodetector under dark and illumination conditions. (c) Photoresponse behavior of the devices. The inset shows the device performance with periodical on/off (30 s/30 s) cycles. (d) Responsivity of the devices biased with 10 V at different wavelengths. (e) Schematic of the energy band structures in the NW network devices with and without light illumination. The energy band structures (both under dark and illumination conditions) are given in short-circuit.

The responsivity of the device over different wavelengths was measured by scanning the light generated from a xenon light source from 220 nm to 400 nm, as shown in Fig. 3d. The device exhibited an increasing response to the incident light when the wavelength is close to 268 nm (the bandgap of ZGO NWs, ~4.6 eV). The photoresponse continued to increase when the wavelength was reduced and reached the maximum value at 250 nm. The cutoff wavelength of the device was ~300 nm. The solar blind (250 nm)–UV (300 nm) rejection ratio was around

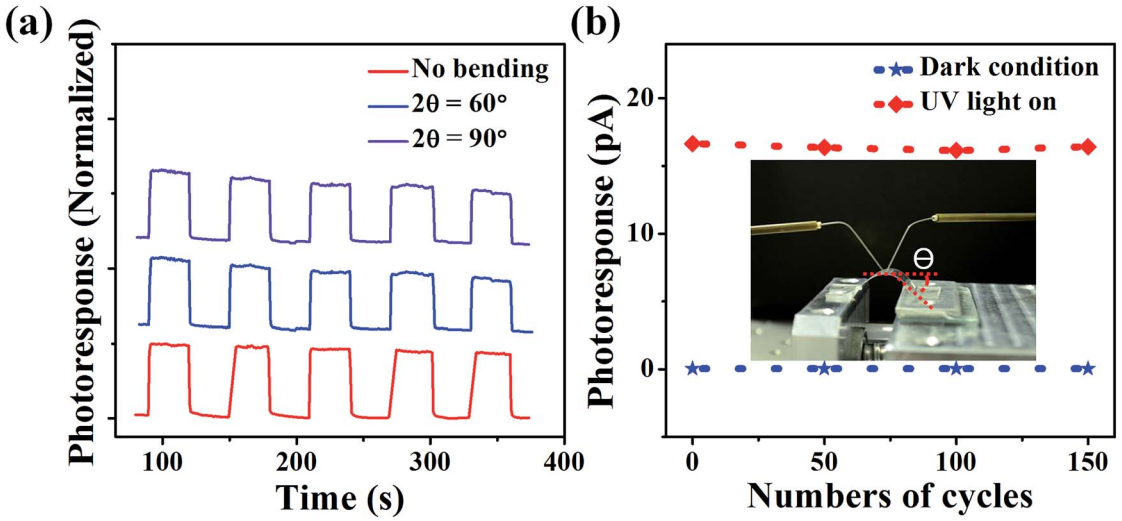

Fig. 4 (a) Performance of the UV-photodetector under bending angles of 0°, 60° and 90°. (b) Photoresponse of the device after different bending cycles in the relaxed state.

1.5×10^4, comparable to the previous report on a single ZGO NW photodetector with a rejection ratio of around 1×10^4 at the wavelengths of 245 nm to 380 nm.[27] However, the single ZGO NW photodetector showed a response to the light illumination until the wavelength increased above 380 nm. The photoresponse of the device in the long wavelength can be attributed to the unintentional doping of the NWs, such as oxygen vacancies and zinc interstices[29] formed during the CVD synthesis process. Electrons can be excited into the shallow dopant levels under the conduction band by the low-energy photons and contribute to the photocurrent.[37,38] However, the energy of these electrons is not sufficient to effectively lower and narrow the energy barrier at the ZGO NW–NW junctions. The existence of the junction barrier provides an additional "filter" to prohibit the transport of electrons excited by the low-energy photons. Consequently, the cutoff wavelength of the ZGO NW network photodetector was further reduced to around 300 nm, making it an ideal candidate for solar-blind detection.

The performance of the NW photodetector was tested under different bending angles as presented in Fig. 4a. The bending angle (2θ) is defined in the inset of Fig. 4b. A decrease of ~12% in the photocurrent was observed at the bending angle of 90° which might be attributed to the tensile strain in the device channels under the bending states. The photodetector possessed good cycling stability in the bending and relaxing test. As shown in Fig. 4b, after bending for 50, 100 and 150 cycles with a bending angle of 90°, the dark current of the device remained almost constant after the bending cycles. The photocurrent showed a slight decrease from 16.6 pA to 16.3 pA after 50 bending cycles and increased again to 16.4 pA after 150 bending cycles. The small photocurrent decrease during the initial bending cycles was probably due to the sliding of NWs and losing interconnection in the NW networks. The sliding might be minor and the interconnection could be occasionally established again after the bending, as shown at the 150th cycle with some increase in the photocurrent. Consequently, small photocurrent fluctuation was observed during the bending test. In brief, the photodetector showed excellent flexibility and stability which were comparable to those reported in previous studies on flexible photodetectors.[39–41] The results suggest that the photodetectors are promising for application in flexible and transparent solar-blind detection.

Conclusions

In conclusion, flexible and transparent photodetectors have been successfully fabricated based on an all-NW device configuration. The device exhibited good transparency of around 80% transmittance in the visible light range and demonstrated high flexibility and stability. The ZGO NWs used for the device fabrication had high purity and good crystallinity which contributed to the huge photoresponse of the device. The photodetectors have a large on/off ratio with the photocurrent reaching 3000 times of the dark current. The network structure in the devices established Schottky barriers between the Ag–ZGO NWs and the NW–NW junction barriers between the interconnected ZGO NWs. These energy barriers enable the improved switching behavior of the photodetectors. The NW–NW junction barriers in the ZGO NWs also help to reduce the cutoff wavelength of the solar-blind detector. The solution processible method developed here is simple and facile which can be easily applied to the fabrication of other flexible and transparent devices.

Acknowledgements

The authors would like to acknowledge the funding support from NTU-A*Star Silicon Technologies Centre of Excellence under the program grant no. 112 3510 0003. The work is also funded by the joint program between Singapore and Japan, with the support from Nanyang Technological University and Japan Society for the Promotion of Science (JSPS).

Notes and references

1 K. Nomura, H. Ohta, A. Takagi, T. Kamiya, M. Hirano and H. Hosono, *Nature*, 2004, **432**, 488.
2 T. Georgiou, R. Jalil, B. D. Belle, L. Britnell, R. V. Gorbachev, S. V. Morozov, Y. J. Kim, A. Gholinia, S. J. Haigh, O. Makarovsky, L. Eaves, L. A. Ponomarenko, A. K. Geim, K. S. Novoselov and A. Mishchenko, *Nat. Nanotechnol.*, 2013, **8**, 100.
3 P. C. Chen, G. Shen, S. Sukcharoenchoke and C. Zhou, *Appl. Phys. Lett.*, 2009, **94**, 043113.
4 J. L. Zhang, C. Wang and C. W. Zhou, *ACS Nano*, 2012, **6**, 7412.
5 M. Razeghi, *Proc. IEEE*, 2002, **90**, 1006.
6 A. A. Hussain, A. R. Pal and D. S. Patil, *Appl. Phys. Lett.*, 2014, **104**, 193301.
7 Y. N. Hou, Z. X. Mei, Z. L. Liu, T. C. Zhang and X. L. Du, *Appl. Phys. Lett.*, 2011, **98**, 103506.
8 W. Tian, T. Y. Zhai, C. Zhang, S. L. Li, X. Wang, F. Liu, D. Q. Liu, X. K. Cai, K. Tsukagoshi, D. Golberg and Y. Bando, *Adv. Mater.*, 2013, **25**, 4625.
9 X. Liu, L. Jiang, X. Zou, X. Xiao, S. Guo, C. Jiang, X. Liu, Z. Fan, W. Hu, X. Chen, W. Lu, W. Hu and L. Liao, *Adv. Mater.*, 2014, **26**, 2919.
10 M. S. Lee, K. Lee, S. Y. Kim, H. Lee, J. Park, K. H. Choi, H. K. Kim, D. G. Kim, D. Y. Lee, S. Nam and J. U. Park, *Nano Lett.*, 2013, **13**, 2814.
11 A. R. Madaria, A. Kumar, F. N. Ishikawa and C. Zhou, *Nano Res.*, 2010, **3**, 564.
12 S. De, T. M. Higgins, P. E. Lyons, E. M. Doherty, P. N. Nirmalraj, W. J. Blau, J. J. Boland and J. N. Coleman, *ACS Nano*, 2009, **3**, 1767.
13 E. C. Garnett, W. S. Cai, J. J. Cha, F. Mahmood, S. T. Connor, M. G. Christoforo, Y. Cui, M. D. McGehee and M. L. Brongersma, *Nat. Mater.*, 2012, **11**, 241.
14 H. Wu, L. Hu, M. W. Rowell, D. Kong, J. J. Cha, J. R. McDonough, J. Zhu, Y. Yang, M. D. McGehee and Y. Cui, *Nano Lett.*, 2010, **10**, 4242.
15 J. V. van de Groep, P. Spinelli and A. Polman, *Nano Lett.*, 2012, **12**, 3138.
16 L. F. Hu, J. Yan, M. Y. Liao, L. M. Wu and X. S. Fang, *Small*, 2011, **7**, 1012.
17 C. Y. Yan and P. S. Lee, *Sci. Adv. Mater.*, 2012, **4**, 241.
18 C. Soci, A. Zhang, X. Y. Bao, H. Kim, Y. Lo and D. L. Wang, *J. Nanosci. Nanotechnol.*, 2010, **10**, 1430.
19 C. Yan, J. Wang, X. Wang, W. Kang, M. Cui, C. Y. Foo and P. S. Lee, *Adv. Mater.*, 2013, **26**, 943.
20 H. Kind, H. Q. Yan, B. Messer, M. Law and P. D. Yang, *Adv. Mater.*, 2002, **14**, 158.
21 C. Soci, A. Zhang, B. Xiang, S. A. Dayeh, D. P. R. Aplin, J. Park, X. Y. Bao, Y. H. Lo and D. Wang, *Nano Lett.*, 2007, **7**, 1003.
22 J. J. Wang, F. F. Cao, L. Jiang, Y. G. Guo, W. P. Hu and L. J. Wan, *J. Am. Chem. Soc.*, 2009, **131**, 15602.
23 J. Wang, C. Yan, W. Kang and P. S. Lee, *Nanoscale*, 2014, **6**, 10734.
24 R. Zou, Z. Zhang, Q. Liu, J. Hu, L. Sang, M. Liao and W. Zhang, *Small*, 2014, **10**, 1848.
25 L. Li, E. Auer, M. Y. Liao, X. S. Fang, T. Y. Zhai, U. K. Gautam, A. Lugstein, Y. Koide, Y. Bando and D. Golberg, *Nanoscale*, 2011, **3**, 1120.
26 L. Li, P. S. Lee, C. Yan, T. Zhai, X. Fang, M. Liao, Y. Koide, Y. Bando and D. Golberg, *Adv. Mater.*, 2010, **22**, 5145.
27 C. Li, Y. Bando, M. Y. Liao, Y. Koide and D. Golberg, *Appl. Phys. Lett.*, 2010, **97**, 161102.
28 C. Yan, N. Singh and P. S. Lee, *Appl. Phys. Lett.*, 2010, **96**, 0531081.
29 J. X. Wang, C. Y. Yan, S. Magdassi and P. S. Lee, *ACS Appl. Mater. Interfaces*, 2013, **5**, 6793.
30 L. Hu, H. S. Kim, J.-Y. Lee, P. Peumans and Y. Cui, *ACS Nano*, 2010, **4**, 2955.
31 Z. Liu, B. Liang, G. Chen, G. Yu, Z. Xie, L. Gao, D. Chen and G. Shen, *J. Mater. Chem. C*, 2013, **1**, 131.
32 Z. Liu, H. T. Huang, B. Liang, X. F. Wang, Z. R. Wang, D. Chen and G. Z. Shen, *Opt. Express*, 2012, **20**, 2982.
33 C. H. Liao, C. W. Huang, J. Y. Chen, C. H. Chiu, T. C. Tsai, K. C. Lu, M. Y. Lu and W. W. Wu, *J. Phys. Chem. C*, 2014, **118**, 8194.
34 T. Y. Wei, C. T. Huang, B. J. Hansen, Y. F. Lin, L. J. Chen, S. Y. Lu and Z. L. Wang, *Appl. Phys. Lett.*, 2010, **96**, 013508.
35 Y. F. Hu, J. Zhou, P. H. Yeh, Z. Li, T. Y. Wei and Z. L. Wang, *Adv. Mater.*, 2010, **22**, 3327.
36 J. Zhou, Y. D. Gu, Y. F. Hu, W. J. Mai, P. H. Yeh, G. Bao, A. K. Sood, D. L. Polla and Z. L. Wang, *Appl. Phys. Lett.*, 2009, **94**, 191103.
37 D. Walker, E. Monroy, P. Kung, J. Wu, M. Hamilton, F. J. Sanchez, J. Diaz and M. Razeghi, *Appl. Phys. Lett.*, 1999, **74**, 762.
38 J. Tang, G. Konstantatos, S. Hinds, S. Myrskog, A. G. Pattantyus-Abraham, J. Clifford and E. H. Sargent, *ACS Nano*, 2008, **3**, 331.
39 L. B. Luo, X. B. Yang, F. X. Liang, J. S. Jie, Q. Li, Z. F. Zhu, C. Y. Wu, Y. Q. Yu and L. Wang, *CrystEngComm*, 2012, **14**, 1942.
40 B. Aksoy, S. Coskun, S. Kucukyildiz and H. E. Unalan, *Nanotechnology*, 2012, **23**, 325202.
41 G. Yu, B. Liang, H. T. Huang, G. Chen, Z. Liu, D. Chen and G. Z. Shen, *Nanotechnology*, 2013, **24**, 095703.